LAPTH 692-98
UM-TH 98-12
CERN-TH/98-244
August 1998

New developments in the $1/N$ expansion and nonperturbative Higgs physics

Thomas Binoth[a] and Adrian Ghinculov[b,c,1]

[a] *Laboratoire d'Annecy-Le-Vieux de Physique Théorique*[2] *LAPP, Chemin de Bellevue, B.P. 110, F-74941, Annecy-le-Vieux, France*

[b] *Randall Laboratory of Physics, University of Michigan, Ann Arbor, Michigan 48109-1120, USA*

[c] *CERN, 1211 Geneva 23, Switzerland*

Abstract

We show in this paper that the $1/N$ expansion is a reliable tool to calculate the properties of a heavy Higgs boson. The 1/N expansion sums up all orders in perturbation theory, and therefore avoids the renormalization scheme dependence of the conventional perturbative approach. It is explained how effects due to the Landau pole of the Higgs sector are isolated and subtracted, and how to perform actual calculations, by computing the Higgs line shape for the processes $f\bar{f} \to H \to ZZ, f'\bar{f}'$ at next-to-leading order in the $1/N$ expansion. The results are compared to the perturbative results to show the agreement between the perturbative and the nonperturbative approach for Higgs masses up to 1 TeV. We conclude that the theoretical predictions for Higgs observables are well under control for the entire kinematical region of the LHC.

1 Introduction

A main goal of future collider physics is to shed light into the electroweak symmetry breaking mechanism. Within the standard model this mechanism is generated by the Higgs

[1] Work supported by the US Department of Energy (DOE)
[2] URA 1436 associée à l'Université de Savoie

sector, leading to gauge invariant mass terms where needed. At the Lagrangean level, this is a gauged linear $O(4)$-symmetric sigma model, spontaneously broken to $O(3)$ by a nonvanishing vacuum expectation value. The mass of the Higgs boson itself is directly related to the corresponding quartic coupling, which implies the nondecoupling property of the Higgs boson. For large Higgs mass one expects large quantum corrections which blow up within the standard perturbative approach.

Within the perturbative approach, a lot of work has been done in the recent years. Many quantum corrections for relevant observables which contain information on the Higgs boson are available [1]. The radiative corrections of enhanced electroweak strength to the decay of the Higgs boson were first derived at one-loop in [2], and at two-loop in [3, 4, 5]. For low values of the Higgs mass the theoretical uncertainty is thus small. For heavier masses the leading order and next-to-leading order results, start to deviate from the NNLO result, inducing theoretical ambiguities. One expects large dependences on the renormalization scheme essentially coming from the truncation of the perturbative series which makes theoretical predictions unreliable. Whereas the perturbative region will be fully covered by LEP, Tevatron and the LHC, it is of special importance to have a good theoretical understanding of the heavy Higgs regime which is also in reach of the LHC. Although the existing experimental data points presently in the direction of a Higgs mass in the perturbative region, one should not forget that these bounds are logarithmically soft, and that the experimental data on $\sin^2\theta_{eff}$ still differ considerably in the high precision measurements at LEP1 and SLC [6]. Moreover, certain two-loop quantities are presently known theoretically only as mass expansions, and given the high statistics of the experiments, this induces rather substantial shifts in the Higgs mass prediction.

Apart from the phenomenological motivation, it is a major challenge to develop and improve calculational methods beyond the standard perturbative approach. A well-known nonperturbative approach are Monte Carlo studies on a lattice. The results of lattice calculations indicate that for Higgs masses beyond ~ 700 GeV one expects large cutoff effects [7]. They stem from the fact that the Higgs sector is not asymptotically free. We advocate another nonperturbative approach, the $1/N$ expansion. There, the quantum correction are ordered by the number of field components [8, 9]. The method was applied to the Higgs sector to leading order a long time ago [10] but the large deviation from standard perturbative results shaded doubts on its validity.

Recently we performed a next-to-leading order calculation of the Higgs propagator, showing at low coupling a remarkable agreement between the NNLO perturbative result and our result [11]. This proved the $1/N$ expansion to be a valuable tool for computing observables beyond the perturbative approach, and for avoiding the truncation of the perturbative series and thus eliminating any renormalization scale dependence.

In this paper we extend the results to the case of three-point functions, which results in a quantitative, nonperturbative understanding of the physical processes $f\bar{f} \to H \to f'\bar{f}', Z_L Z_L$. It was tried to make the computation as transparent as possible to convince the reader that the method is conceptually well settled and practicable, though some amount of numerical work is unavoidable, which on the other hand is common to the calculation of higher-order finite momentum Green functions in massive theories.

After some preliminaries, where we remind the LO results and the issue of the tachyon of the $1/N$ approach, we show how one obtains a well defined, tachyon free representation

of Green functions. An ultraviolet subtraction scheme is defined in terms of an order $1/N$ counterterm Lagrangean. Then, the finite and tachyon free Green functions are expressed in form of multiloop graphs made out of dressed propagators. These can be reduced to two-dimensional integrals over dressed propagators and form factors. Then we describe how to perform the remaining integrations numerically, to obtain the final results for the two- and three-point functions. We show and discuss our nonperturbative result for the Higgs line shapes in two physical scattering processes, and compare to the perturbative result. After this discussion, we summarize the conclusions of the paper.

2 Preliminaries

In this section we review the leading order result for fixing our notations, and discuss the structure of the counterterms which absorb the ultraviolet divergencies at leading and next-to-leading order.

Because we are interested in the effects of a heavy Higgs boson, we neglect all the gauge couplings and also the higher order corrections in the Yukawa couplings. Thus, the starting point for the $1/N$ expansion in a scalar theory is given by an $O(N)$-symmetric ϕ^4 theory:

$$\mathcal{L} = \frac{1}{2}\,\partial_\nu \vec{\phi}_0 \partial^\nu \vec{\phi}_0 - \frac{1}{2}\mu_0^2\,\vec{\phi}_0^{\,2} - \frac{\lambda_0}{4!N}(\vec{\phi}_0^{\,2})^2 \tag{1}$$

Here $\vec{\phi}_0$ is a N-component vector and μ_0, λ_0 are bare coupling constants indicated by the subscript zero. Because we want to focus on the spontaneously broken case, we rewrite it as

$$\mathcal{L} = \frac{1}{2}\,\partial_\nu \vec{\phi}_0 \partial^\nu \vec{\phi}_0 - \frac{\lambda_0}{4!N}(\vec{\phi}_0^{\,2} - N v_0^2)^2 \tag{2}$$

$N v_0^2 = -6N\mu_0^2/\lambda_0$ is the bare vacuum expectation value of $\vec{\phi}^{\,2}$. The symmetry of the ground state is broken down to $O(N-1)$, which amounts to the presence of $N-1$ massless Goldstone bosons (GBs), $\pi_{i=1,\ldots,N-1}$, and a Higgs particle h, of mass $m_h^2 = \lambda_0 v_0^2/3$. In the case $N = 4$, the GBs are related to the longitudinal degrees of freedom of the vector bosons W_L, Z_L by the equivalence theorem.

To overcome the combinatorial difficulties of multi-loop calculations, we use a well-known auxiliary field formalism [8]. We add to the Lagrangean the following expression, which becomes identically zero when one uses the equations of motion:

$$\mathcal{L}_\chi = \frac{3N}{2\lambda_0} Z_\kappa \Big[\chi_0 - \frac{\lambda_0}{6N}(\vec{\phi}_0^{\,2} - N v_0^2)\Big]^2. \tag{3}$$

Z_κ is an arbitrary Lagrange multiplier. One additionally has the freedom to replace χ_0 by $\alpha\chi_0 + \beta$, where α, β are some constants, without changing the equations of motion. These constants correspond to a χ vacuum expectation value and a wave function renormalization. We introduce renormalized quantities in the following way:

$$\phi_0 = \sqrt{Z_\phi}\,\phi = \sqrt{Z_\phi}(\vec{\pi}, \sqrt{\frac{Z_h}{Z_\phi}}\sigma), \quad v_0 = \sqrt{Z_\phi} Z_v v, \quad \lambda_0 = \frac{Z_\lambda}{Z_\phi^2}\lambda, \quad \chi_0 = \frac{Z_\chi}{Z_\phi}(\chi + V_\chi) \qquad (4)$$

From the discussion above it is clear that only Z_ϕ, Z_h, Z_λ and Z_v are renormalization constants in the usual sense. The other can be chosen arbitrarily as long as the choice is consistent. Their introduction will turn out to be useful for the renormalization of functions which contain auxiliary particles as external legs. The Lagrangean is now of the form:

$$\begin{aligned} \mathcal{L} &= \frac{c_0}{2}\partial_\nu\vec{\phi}\partial^\nu\vec{\phi} + c_1 N v^2\chi + \frac{c_2}{2}\frac{Nv^2}{m_h^2}\chi^2 \\ &\quad -\frac{c_3}{2}\chi(\vec{\phi}^2 - Nv^2) - \frac{c_4}{2}(\vec{\phi}^2 - Nv^2) - \frac{c_5}{8}\frac{m_h^2}{Nv^2}(\vec{\phi}^2 - Nv^2)^2 \end{aligned}$$

with

$$\vec{\phi} = (\vec{\pi}, c_6\,\sigma + \sqrt{N}v) \quad . \qquad (5)$$

Note that a mixing between χ and σ takes place. We see that the expression contains — up to a trivial surface term $\Box\chi$ — all possible field combinations of dimension four which are built out of an $O(N)$ vector and a dimension two singlet field allowed by Lorentz invariance and the $O(N)$ symmetry. The vacuum expectation value of the Higgs reduces the symmetry as usual to $O(N-1)$. The constants $c_{i=0,\ldots,6}$ are expressible in terms of the above renormalization constants.

$$\begin{array}{lll} c_0 = Z_\phi & c_1 = Z_\chi Z_\kappa(\frac{Z_\chi V_\chi}{Z_\lambda m_h^2} + \frac{Z_v^2-1}{2}) & c_2 = \frac{Z_\kappa Z_\chi^2}{Z_\lambda} \\ c_3 = Z_\chi Z_\kappa & c_4 = Z_\chi Z_\kappa V_\chi & c_5 = (1-Z_\kappa)Z_\lambda \\ c_6 = \sqrt{Z_h/Z_\phi} & & \end{array} \qquad (6)$$

These constants define a redundant counterterm structure of the theory, and are fixed by imposing conditions on one-particle irreducible Green functions. Whereas some are necessary to absorb the divergencies occurring in physical processes, other can be adjusted to make subtractions on Green functions containing auxiliary fields as external legs. Clearly all these subtractions have to be consistent with each other. In order to determine the renormalization constants, the quantum corrections to the tree level Green functions have to be calculated up to a given order, and have to be related to the counterterms by a renormalization scheme.

In perturbation theory the occurring renormalization scheme dependence is proportional to some power of the coupling constant, and namely one order higher than the loop order in which the process is calculated. Thus it is enhanced in the case of strong coupling. It is a crucial point that this is not the case in the $1/N$ expansion. Once the relations between a set of observables and the Green functions are fixed, all further predictions are exact, up to unevaluated powers of $1/N$. A change of the ultraviolet subtraction point μ^2 (see below) is compensated by a change in λ. Thus it does not effect any observable prediction, being merely a reparameterization of the theory.

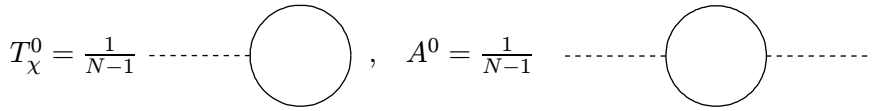

Figure 1: *Leading order tadpole and self-energy graphs.*

Before describing the computation of the Higgs propagator in next-to-leading order in $1/N$, we would like to repeat the leading order results to set the stage for the next step. To order $(1/N)^0$ the quantum corrections are simply the sum of all graphs containing arbitrary numbers of external χ legs attached to a GB loop. The sum can be carried out and a simple closed expression for the resulting effective potential can be found [8]. The only divergent graphs are a χ tadpole and a momentum dependent χ self-energy graph shown in figure 1. Both divergencies can be absorbed into Z_v and Z_λ, or in other words, into the coupling constants of the theory. No other renormalization constant is involved. Whereas the observable vev is defined by the ground state of the theory — resulting in an observable vector boson mass if one couples the model to a gauge theory — the value of λ can be fixed by a measurement of the Higgs mass. In terms of the introduced renormalization constants, one has:

$$Z_v^2 = 1 - 2\,T^0_\chi, \quad 1/Z_\lambda = 1 - \lambda A^0(-\mu^2)/3, \quad Z_\phi = Z_h = Z_\chi = Z_\kappa = 1, \quad V_\chi = 0 \quad . \tag{7}$$

The integrals which correspond to the leading order corrections are trivial. Absorbing combinatorial factors in the expressions, one finds in dimensional regularization:

$$\begin{aligned} A^0(s) &= -\frac{1}{32\pi^2}\log(-s/\Lambda^2) + \frac{\text{const.}}{\epsilon} + \text{const.'} \\ T^0_\chi &= 0 \end{aligned} \tag{8}$$

Defining an energy dependent Higgs mass by $m^2(s) = v^2\lambda(s)/3$, where $1/\lambda(s) = 1/\lambda + (\alpha_0(s) - \alpha_0(\mu^2))/3$, one gets an expression for the matrix of two-point functions. Its inverse defines the dressed propagators to leading order. μ is the renormalization scale. The resulting propagators are found to be:

$$\begin{aligned} D_{hh} &= \frac{i}{s - m^2(s)} \\ D_{h\chi} &= \frac{i}{\sqrt{N}v}\frac{m^2(s)}{s - m^2(s)} \\ D_{\chi\chi} &= \frac{i}{Nv^2}\frac{s\,m^2(s)}{s - m^2(s)} \\ D_{\pi_l\pi_k} &= \frac{i}{s}\,\delta_{lk} \end{aligned} \tag{9}$$

The GB propagator is not influenced at leading order. Clearly the same results can be obtained without the auxiliary field. The dressed χ propagator corresponds to a geometric

series of loop graphs [10]. Note that the propagators contain an imaginary part for physical, timelike momenta, which describes Higgs decay into Goldstone bosons. To keep the pole on the correct Riemann sheet one has to use the $i\epsilon$ prescription in the logarithm of the s-dependent mass:

$$\frac{1}{m^2(s)} = \frac{1}{m_h^2} - \frac{1}{32\pi^2 v^2} \log(-\frac{s}{\mu^2} - i\epsilon) \tag{10}$$

For spacelike momenta, a Landau pole occurs at the scale:

$$\Lambda_L = \mu \exp\left[\left(\frac{4\pi v}{m_h}\right)^2\right] \quad . \tag{11}$$

Since $m^2(s)$ is negative beyond the Landau scale Λ_L, all these propagators have an extra pole for a spacelike momentum $s = -\Lambda^2_{T(achyon)}$ which is defined by the equation:

$$\Lambda_T^2 + m^2(-\Lambda_T^2) = 0\,, \qquad \Lambda_T^2 > 0 \qquad . \tag{12}$$

There is a tendency to discard non asymptotically free theories as fundamental theories. The occurrence of the tachyon in the sigma model is widely believed to be an indication of an ill-defined quantum field theory. However, to or knowledge there is so far no rigorous proof thereof. We will show in the next section that the tachyon is technically an artifact of perturbation theory and can by no means be considered an inconsistency of the model. Apart from these issues, it is natural to ask for higher order effects. How to go beyond the leading order in $1/N$ is directly related to the tachyon problem, because on has to integrate over graphs built out of tachyon contaminated propagators. A method to treat this is given below. Such a procedure is touching the aspects of the theory which cannot be investigated by Feynman diagrams, even summed up to all orders. In this sense any tachyonic regularization is modeling either effects from a more fundamental theory containing the Higgs sector as a low energy limit, or a certain type of nonperturbative effects within the Higgs sector itself. Our nonperturbative treatment of the sigma model is independent of an interpretation either as an effective theory or as a fundamental theory, and we will make no assumption in this direction in this paper.

3 Calculation

In this section we explain the necessary steps to calculate the NLO corrections to the processes $f\bar{f} \to H \to Z_L Z_L, W_L W_L, f'\bar{f}'$ in the $1/N$ expansion. In the case of longitudinal vector boson decay modes, we calculate the processes by using the equivalence theorem. Therefore we repace the longitudinal vector bosons by the corresponding would-be Goldstone bosons z and w. To this end one has to know the two- and three-point functions to that order. To get a physically meaningful quantity one has to define a perturbative renormalization procedure to deal with the usual divergencies. On the other hand one has to define a scheme to treat the tachyon which is a perturbative artifact of the leading order calculation. We have seen that the infinite series of Feynman diagrams shows up in the propagators as a momentum dependent mass producing a tachyon pole. The dressed

propagators in eq. 9 are, together with the occurring vertices and the counterterms defined in eqn. 5, the building blocks of the diagrams which describe the next-to-leading order effects. To leading order, only GB propagators appear as internal lines. It is crucial for the simplicity of the calculation that, with the help of the auxiliary field χ, the next-to-leading order contributions of the $1/N$ expansion to the Higgs propagator can be depicted by a small number of graphs.

In the following, a tachyonic regularization will be defined. Then the diagrammatical part of the calculation will be given together with the renormalization procedure. The subtractions will be explained in detail for the relevant multi-loop graphs, and the finite, tachyon-free quantum corrections to the two- and three-point functions will be derived. They will be represented as two-fold integrals. Finally the remaining two dimensional integration is performed numerically, which gives quantitatively the propagator and vertex corrections.

3.1 Tachyon subtraction

Before starting the calculation, we introduce a tachyon-free representation for the occurring propagators [11]. Assuming that its occurrence is not due the failure of the theory under consideration, but of the intermediary expansion technique used [11], it is reasonable to circumvent the ill-defined part by an adequate subtraction of the tachyonic pole. If the ϕ^4 theory is only describing a low energy effective theory, some physics at a higher scale will cure the problem. It is clear that *a priori* the tachyon regularization is not unique, and one has to pay the price in the form of an additional ambiguity. We modify the propagators in eq. 9 by the following subtraction of the tachyonic pole, which is the minimal way of eliminating the tachyonic pole:

$$\begin{aligned} \frac{1}{s-m^2(s)} &\rightarrow \frac{1}{s-m^2(s)} - \frac{1}{s+\Lambda_T^2}\,\kappa \\ \frac{m^2(s)}{s-m^2(s)} &\rightarrow \frac{m^2(s)}{s-m^2(s)} + \frac{\Lambda_T^2}{s+\Lambda_T^2}\,\kappa \end{aligned} \tag{13}$$

$\kappa = 32\pi^2 v^2/(32\pi^2 v^2 + \Lambda_T^2)$ is just the residuum of the tachyonic pole. To get a quantitative feeling for the size of the subtracted terms we give some values of the appearing constants in table 1. It is clear from eq. 10 that only a pair of parameters m_h, μ defines a physical situation. We related μ to the position of the Higgs pole in the complex plane, $M_{Pole} - i\Gamma_{Pole}/2$, by the relation $\mu^2 = M_{Pole}^2 + \Gamma_{Pole}^2/4$ [10]. Its position is also shown in the table. Near the Higgs resonance, the residuum of the tachyonic pole is a measure for the quantitative influence of the tachyonic regularization. Any amplitude will be modified there by terms proportional to κ. The perturbative expansion of these terms vanishes identically.

Another strategy to treat the tachyon issue would be the introduction of a momentum cutoff [12]. Such a cutoff has to be under the tachyon scale, and destroys the gauge invariance in the gauged model. On the contrary, our tachyonic regularization preserves the symmetry of the model in all orders of perturbation theory.

m_h	M_{Pole}	Γ_{Pole}	Λ_L	Λ_T	κ
0.20	0.20	5.3×10^{-3}	1.7×10^{25}	1.7×10^{25}	1.6×10^{-50}
0.40	0.40	0.04	1.2×10^{6}	1.2×10^{6}	0.1×10^{-6}
0.60	0.59	0.15	0.5×10^{3}	0.5×10^{3}	0.6×10^{-3}
0.80	0.74	0.34	3.2×10	3.2×10	4.7×10^{-3}
1.00	0.83	0.58	9.64	9.88	4.7×10^{-2}
1.20	0.87	0.82	5.03	5.45	0.14
1.40	0.86	1.00	3.36	3.93	0.24
1.60	0.84	1.11	2.57	3.23	0.31
1.80	0.82	1.19	2.12	2.85	0.37
2.00	0.81	1.24	1.85	2.62	0.41

Table 1: *Information on the physical and the tachyonic pole at leading order. The parameter m_h is related to the physical pole in the way explained in the text. The dimensionful quantities are in TeV.*

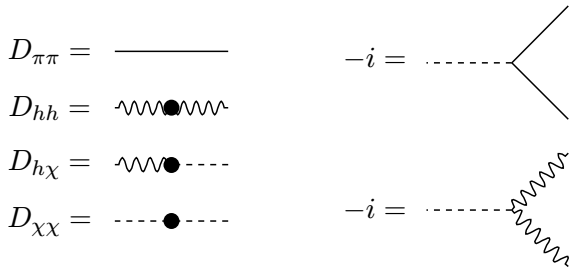

Figure 2: *Feynman rules. The dot indicates the dressed, tachyon free propagators. The counterterms are defined by eq. 14.*

3.2 Diagrammatics

The Feynman rules for the next-to-leading order calculation contain the full LO propagators given above in eq. 9 and the interaction terms defined in eqs. 5. The propagators are understood as tachyonicaly regulated by the prescription of eqs. 13. Thus the diagrammatical part of the calculation is settled. The Feynman rules are given in figure 2.

The dot indicates the dressed propagators stemming from the leading order calculation. We now fix the counterterms. Considering the values of the leading order renormalization constants, we write $Z_\kappa = 1 - \kappa/N$, $Z_\phi = 1 + z_\phi/N$, $Z_h = 1 + z_h/N$, $Z_v^2 = 1 + 2z_v/N$, $V_\chi = v_\chi/N$, $1/Z_\lambda = 1 - z_\lambda/N$, $Z_\chi = 1 + z_\chi/N$. The LO counterterm is already absorbed in the definition of the dressed propagators. The NLO counterterm Lagrangean is expressible in terms of these new variables:

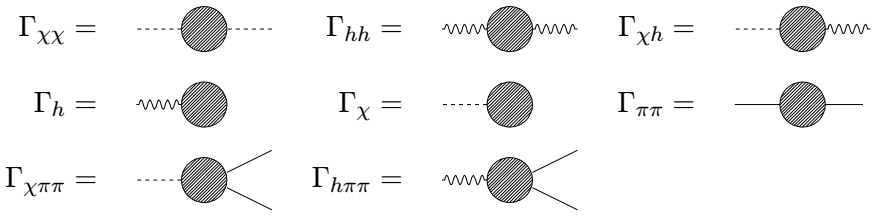

Figure 3: *Relevant two- and three-point functions to be calculated.*

$$\begin{aligned}\mathcal{L}_{counterterm} &= \frac{1}{N}\Bigg[\frac{z_\phi}{2}\partial_\nu\vec{\phi}\partial^\nu\vec{\phi} + Nv^2\Big(\frac{v_\chi}{m_h^2}+z_v\Big)\chi + \frac{Nv^2}{m_h^2}\left(2z_\chi-\kappa-z_\lambda\right)\frac{\chi^2}{2} \\ &\qquad -\frac{z_\chi-\kappa}{2}\chi(\vec{\phi}^2-Nv^2) - \frac{v_\chi}{2}(\vec{\phi}^2-Nv^2) - \frac{m_h^2\kappa}{8Nv^2}(\vec{\phi}^2-Nv^2)^2\Bigg] \\ \vec{\phi} &= (\vec{\pi}, \sqrt{\frac{Z_h}{Z_\phi}}\sigma + \sqrt{N}v) \end{aligned} \tag{14}$$

As we will see below, the NLO corrections are expressible in form of multi-loop diagrams made out of the dressed propagators. The counterterms in eq. 14 will allow to make subtractions of subgraphs inside these diagrams which is the motivation for our redundant renormalization formalism.

The relevant two- and three-point functions are shown in figure 3. Their actual form in terms of graphs will be shown below.

The counterterms are fixed by some renormalization conditions. Two conditions are already dictated by the cancellation of tadpole contributions. Further conditions may be imposed on one-particle irreducible two- and three-point functions. We consider the following conditions:

$$\Gamma'_{\pi\pi}(0) = \Gamma'_{hh}(0) = \frac{m_h^2}{Nv^2}\Gamma_{\chi\chi}(\mu^2) = \frac{-1}{\sqrt{N}v}\Gamma_{h\chi} = 1, \quad \Gamma_\chi = \Gamma_\sigma = \Gamma_{h\pi\pi}(0,0) = 0 \tag{15}$$

These conditions define a renormalization scheme. Otherwise, all possible counterterms are fixed by the symmetry of the counterterm Lagrangean of eq. 14. Whenever possible we set the renormalization scale to zero, because the multiloop counterterms turn out to be analytically simpler, as will become clear later. When the subtraction point μ cannot be set to zero because of infrared problems, we combined the multiloop graph with the corresponding counterterms at an Euclidian μ and such that the sum is free of the infrared singularity, and afterwards we took the limit $\mu \to 0$.

The list of needed graphs is given in figure 4. One finds these graphs by usual power counting in $1/N$. A detailed discussion of their computation will follow in the next subsection where the analytical part of the calculation is done. The renormalization constants can

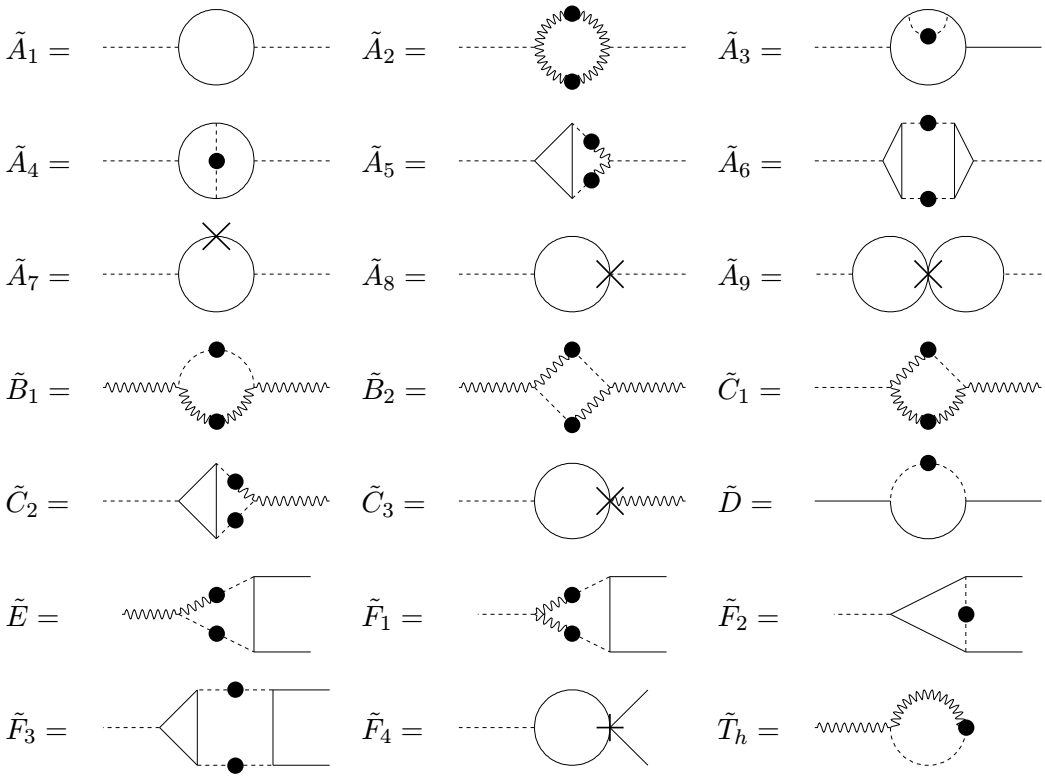

Figure 4: *List of occurring graphs to order* $1/N$

be determined through the scheme of eq. 15 in terms of vacuum graphs of the type given in figure 4. By using

$$\begin{aligned}\tilde{A}(\mu^2) &= -\tilde{A}_1(-\mu^2)/2 + \tilde{A}_2(0)/2 - \tilde{A}_3(0) - \tilde{A}_4(0)/2 - \tilde{A}_5(0) + \tilde{A}_6(0)/2 \\ &\quad +\tilde{A}_7(-\mu^2) - \tilde{A}_8(-\mu^2) + \tilde{A}_9(-\mu^2)/4 \\ \tilde{C}(\mu^2) &= \tilde{C}_1(0) - \tilde{C}_2(0) + \tilde{C}_3(-\mu^2)\end{aligned}$$

one finds

$$\begin{array}{lll} z_\phi = -v^2\tilde{D}'(0) & z_h = -v^2\tilde{B}_1'(0) & z_v = -\tilde{T}_\chi - \frac{v^2\tilde{T}_h}{m_h^2} \\ z_\chi = \frac{2v^2}{m_h^2}\tilde{B}_2(0) + \tilde{C}(0) & \kappa = \frac{2v^2}{m_h^2}\tilde{B}_2(0) & v_\chi = v^2\tilde{T}_h \\ z_\lambda = \frac{m_h^2}{v^2}\tilde{A}(\mu^2) + \frac{2v^2}{m_h^2}\tilde{B}_2(0) + 2\tilde{C}(\mu^2) & & \end{array} \tag{16}$$

Note that the occurring expressions can be expanded in λ. This provides the connection to the standard loop expansion, and allows to check the consistency of the renormalization procedure to any order diagramatically.

3.3 Analytical framework

In order to keep our expressions compact, we introduce the following notations:

$$g(s) = \frac{1}{s - m^2(s)}\,, \quad f(s) = \frac{m^2(s)}{s - m^2(s)} \tag{17}$$

We further do not write down explicitly the tachyonic regularization of the propagators, but we understand that the tachyonic pole has to be subtracted according to the discussion of the previous section before numerical integration is performed.

To obtain compact formulae for the occurring $1/N$ graphs, we use in the following the massless scalar one-loop three- and four-point functions as building blocks. Their explicit expressions [13, 14] are listed in the appendix. With the help of these functions, the two- and three-loop topologies can be cast into the form of two-fold integrals. The $1/N$ graphs which we need correspond to the following list of dimensionless integrals, where $r = (q + k)$ and we use the notation $dQ = \frac{d^4q}{(2\pi)^4 i}$. k and μ stand for a timelike and spacelike four-vector respectively, and l_μ is a lightlike four-vector corresponding to on-shell GBs. To work with dimensionless quantities, we divide the $1/N$ graphs by appropriate factors of v. We distinguish ultraviolet subtracted graphs from unsubtracted ones by a tilde.

3.3.1 One-loop topologies

$$\tilde{T}_h = \frac{1}{v^4}\int dQ\, f(q^2) \tag{18}$$

$$A_1 = -\int dQ \frac{1}{q^2}\left(\frac{1}{r^2} - \frac{1}{(q+\mu)^2}\right) = \frac{1}{(4\pi)^2}\log\Big(\frac{-k^2}{\mu^2}\Big) \tag{19}$$

$$
\begin{aligned}
A_2 &= \int dQ g(q^2)\Big[g(r^2) - g(q^2)\Big] && (20)\\
B_1 &= \frac{1}{v^4}\int dQ q^2 f(q^2)\Big[g(r^2) - g(q^2) - k^2\frac{d}{dk^2}|_{k^2=0}\frac{1}{r^2}\Big] && (21)\\
B_2 &= \frac{1}{v^2}\int dQ f(q^2)\Big(f(r^2) - f(q^2)\Big) && (22)\\
C_1 &= \frac{1}{v^2}\int dQ f(q^2)\Big[g(r^2) - g(q^2)\Big] && (23)\\
D &= \frac{1}{v^4}\int dQ q^2 f(q^2)\left(\frac{1}{r^2} - \frac{1}{q^2} - k^2\frac{d}{dk^2}|_{k^2=0}\frac{1}{r^2}\right) && (24)\\
E &= \frac{1}{v^2}\int dQ\left[\frac{q^2}{(q+l)^2}f(q^2)f((q-k)^2) - f^2(q^2)\right] && (25)\\
F_1 &= \frac{1}{v^2}\int dQ f(q^2)\left[\frac{q^2}{(q-l)^2(q-l+k)^2} - \frac{1}{q^2}\right] && (26)\\
F_2 &= \frac{1}{v^2}\int dQ\left[\frac{q^2}{(q+l)^2}f(q^2)f((q-k)^2) - f^2(q^2)\right] && (27)\\
& && (28)
\end{aligned}
$$

All necessary counterterms for the subtractions appear in the counter Lagrangean of eq. (14), as one can show by using the relations $\tilde{T}_h = \tilde{D}(0) = \tilde{B}_1(0) - \tilde{B}_2(0)$, $\tilde{F}_1(0) + \tilde{F}_2(0) = \tilde{C}_1(0)$. For convenience we define $B_1(s) = \tilde{B}_1(s) - \tilde{B}_1(0) - s\tilde{D}'(0)$ because we will not explicitly need the wave function renormalization of the Higgs boson which is related to $\tilde{B}'$. Note that $\tilde{T}_h = \tilde{D}(0)$ is a necessary consistency condition to keep the GBs massless after summing the perturbative series. This holds independently of the tachyon. One can check that to render $\tilde{B}_1$ and $\tilde{D}$ finite, one subtraction is already sufficient. This means that one gets an ultraviolet convergent wave function renormalization constant, in contrast to usual perturbation theory. Also note that graphs like $\tilde{B}_2$, with two momentum dependent masses in the numerator, have an extra suppression factor of $1/log^2(q^2)$ in the ultraviolet, which leads to a convergent integral[3]. The summation of all loop graphs thus improves the UV behaviour. This ultraviolet screening is a remarkable feature of the nonperturbative $1/N$ expansion.

3.3.2 Higher-loop topologies

For the higher-loop topologies one has to subtract the subgraphs first. The necessary subtractions are most transparent in a graphical representation. We have collected them in figure 5.

The reader can check that the counterterms defined in eq. 14 correspond to sums of boxed graphs. For the three-point counterterms, this is shown in figure 6.

Note that the sum of the $1/N$ graphs and counterterms for a given topology gives an infrared finite result. Thus, to derive the following formulae, it is necessary to introduce an infrared regulator for the individual terms which cancels in the final sum. As stated above,

[3]The integral converges as $1/\log\Lambda_{cutoff}$

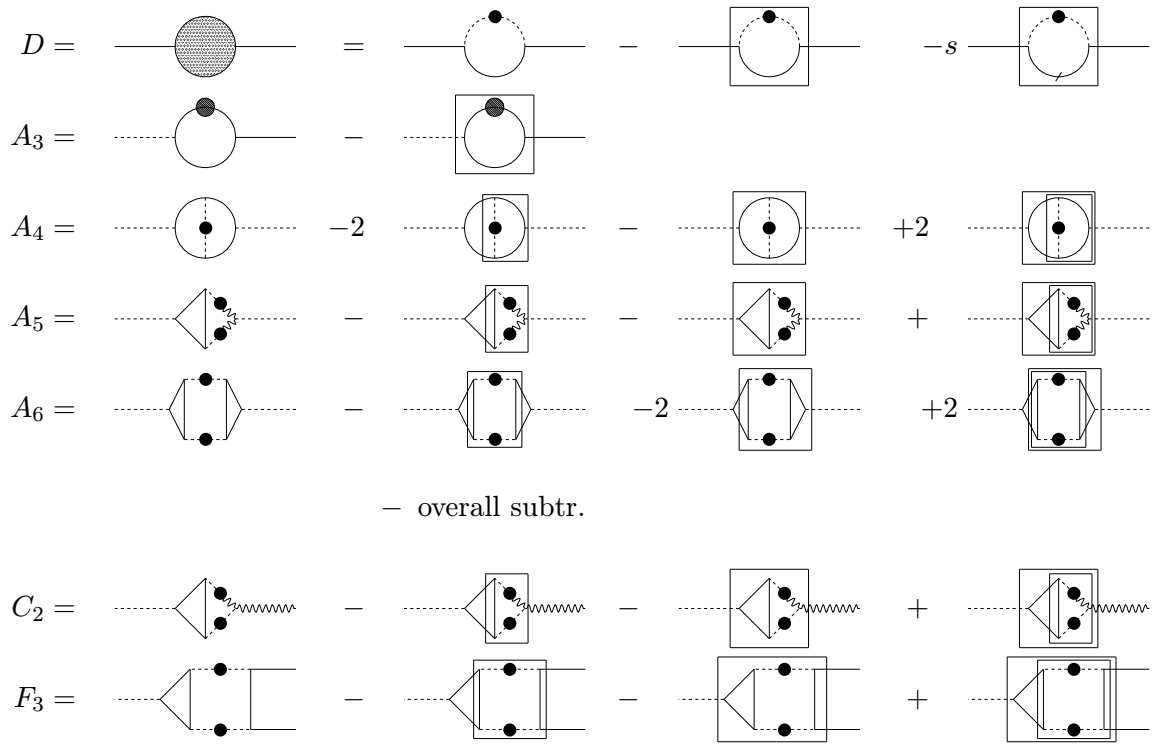

Figure 5: *Subtraction scheme of the higher loop topologies. In the countergraph of D, the dash stands for differentiation with respect to the external momentum and the box means that the contained subgraphs have to be evaluated at vanishing external momenta.*

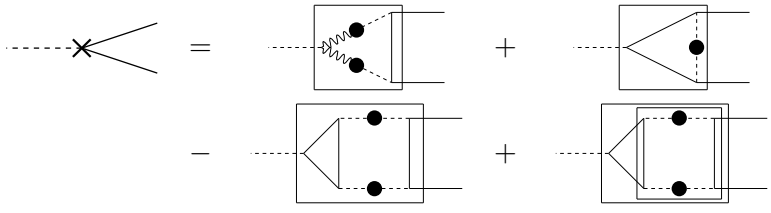

Figure 6: *Graphical representation of the* $\Gamma_{\chi\pi\pi}$ *counterterm.*

we are using analytical expressions for the massless three- and four- point functions, C_0, D_0, which are given in an appendix for completeness.

$$\begin{aligned}
A_3 &= \frac{1}{v^2}\int dQdP \frac{f(q^2)q^2}{(p^2)^2}\left[\frac{1}{(p+k)^2}-\frac{1}{q^2}\right]\left[\frac{1}{(p+q)^2}-\frac{1}{p^2}-\frac{q^2}{(p^2)^2}\Big(1-\frac{4(p\cdot q)^2}{p^2q^2}\Big)\right] \\
&= \frac{1}{v^2}\int dQ \frac{f(q^2)}{q^2(4\pi)^2}\left[1-\frac{2(q\cdot k)^2}{q^2k^2}-\frac{q^2}{k^2}\log\Big(\frac{r^2}{q^2}\Big)\right] \\
A_4 &= \frac{1}{v^2}\int dQ \frac{f(q^2)}{q^2}\Bigg](q^2)^2 D_0(k,q,-k)-\frac{1+\log(\frac{q^2}{k^2})}{8\pi^2}\Bigg] \\
A_5 &= \frac{1}{v^2}\int dQ \left[f(r^2)f(q^2)C_0(k,q)-f^2(q^2)\frac{2+\log(\frac{q^2}{k^2})}{(4\pi)^2q^2}\right] \\
A_6 &= \frac{1}{v^4}\int dQ \left[r^2q^2f(r^2)f(q^2)C_0^2(k,q)-f^2(q^2)\left(\frac{2+\log(\frac{q^2}{k^2})}{(4\pi)^2}\right)^2\right] \\
C_2 &= \frac{1}{v^2}\int dQ \left[q^2f(r^2)f(q^2)C_0(k,q)-f^2(q^2)\frac{2+\log(\frac{q^2}{k^2})}{(4\pi)^2}\right] \\
F_3 &= \frac{1}{v^4}\int dQ \left[f(r^2)f(q^2)C_0(k,q)\frac{r^2q^2}{(q-l)^2}-f^2(q^2)\frac{2+\log(\frac{q^2}{k^2})}{(4\pi)^2}\right]
\end{aligned} \tag{29}$$

We will need in the following sums of these expressions taking into account combinatorial factors and signs.

$$\begin{aligned}
A(s) &= -\frac{1}{2}A_1(s)+\frac{1}{2}A_2(s)-A_3(s)-\frac{1}{2}A_4(s)-A_5(s)+\frac{1}{2}A_6(s) \\
B(s) &= B_1(s)+B_2(s) \\
C(s) &= C_1(s)-C_2(s) \\
F(s) &= F_1(s)+F_2(s)-F_3(s)
\end{aligned} \tag{30}$$

The functions A, B, C, D, E, F are integrals over Minkowski space, parameterized by $q_\nu = (q_0, \rho\vec{n})$. After performing the angular integration, the number of integrations can be reduced to two. Choosing the timelike momentum as $k_\nu = (\sqrt{s}, \vec{0})$, it is obvious that the integrals which belong to two-point functions are isotropic. For the three-point function with on-shell GBs, one has a second timelike four-vector $l_\nu = (1,0,0,1)\sqrt{s}/2$. Explicitly, one finds for the angular integration:

$$\begin{aligned}
\int \frac{d\Omega}{4\pi}\frac{1}{(q-l)^2} &= \frac{1}{2\rho\sqrt{s}}\log\left[\frac{q^2+\sqrt{s}(q_0+\rho)}{q^2+\sqrt{s}(q_0-\rho)}\right] \\
\int \frac{d\Omega}{4\pi}\frac{1}{(q-l)^2(q-l+k)^2} &= \frac{1}{4q_0\rho s}\log\left[\frac{(q^2)^2-s(q_0-\rho)^2}{(q^2)^2-s(q_0+\rho)^2}\right]
\end{aligned} \tag{31}$$

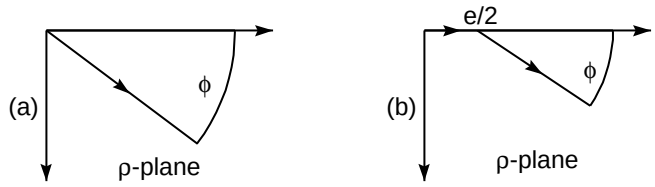

Figure 7: *Integration contours for the numerical integration of the (a) two- and (b) three-point functions.* $e = \sqrt{s}$.

Thus we end up with two-dimensional integral representations for the relevant graphs contributing to the processes we look for. In principle the q_0 integration is also manageable by complex rotation, but one has to take great care because of the complicated singularity and cut structure of the integrands. We proceed numerically in the following.

3.4 Numerical calculation of the diagrams

The numerical problems encountered in the calculation of the needed diagrams are twofold. First of all, one faces convergence problems due to the physical particle poles. Although the massive propagators have a finite width in our case, one still has to use a Wick rotation to get a fast numerical convergence. To do the two dimensional numerical integration:

$$\int_{-\infty}^{\infty} dq_0 \int_{0}^{\infty} d\rho \rho^2 f(q_0, \rho)$$

one chooses the contours in the complex ρ plane to avoid the cuts of the logarithms and to stay away from the poles. They are shown in figure 7. For the two-point functions, a simple rotation $\rho \to \rho \exp(-i\phi)$ leads to a smooth integrand (a), for the three point function one has to avoid also the cut of the logarithms present in eq. 31 (b). No singularity and cut is crossed for any $\phi \in (0, \pi/2)$. The independence of the numerical result of ϕ serves as a test of the stability of the integration.

The procedure gives fast and accurate results as long as the integrand is well behaved at infinity. This is the second problem of the numerical part of the calculation. Usually in loop calculations one is able to separate the UV divergent part by evaluating the Feynman graphs in $4 + \epsilon$ dimensions. The regularization leads to manifestly finite integrands. If, as in our calculation, the regularization has to be done by subtracting divergent counterterms from divergent graphs, the numerical situation is more delicate because of cancellations. To ensure numerical ultraviolet stability, it is necessary to arrange the integrand in such a way that as many cancellations as possible are manifest. For the integrations we used adaptive, deterministic Fortran routines.

4 The results

To derive physical amplitudes, we collect our results for the two- and three- point functions. For the renormalized two-point functions one finds the following expressions:

$$\begin{aligned}
\Gamma_{\{h,\chi\}}(s) &= \begin{bmatrix} \Gamma_{\chi\chi} & \Gamma_{h\chi} \\ \Gamma_{h\chi} & \Gamma_{hh} \end{bmatrix} = \begin{bmatrix} \frac{Nv^2}{m^2(s)} + A(s) & -\sqrt{N}v\left(1-\frac{C(s)}{N}\right)\sqrt{\frac{Z_h}{Z_\phi}} \\ -\sqrt{N}v\left(1-\frac{C(s)}{N}\right)\sqrt{\frac{Z_h}{Z_\phi}} & \left(s+\frac{v^2B(s)}{N}\right)\frac{Z_h}{Z_\phi} \end{bmatrix} \\
\Gamma_{\pi_k\pi_l}(s) &= s\left[1+\frac{v^2}{N}D(s)\right]\delta_{kl}
\end{aligned} \tag{32}$$

The leading order contribution is contained in the momentum dependent mass. The GBs, labeled by $k, l \in \{1, \ldots, N-1\}$, do not mix with the χ, h fields. The wave function renormalization constants appear because of our definition of B_1. As mentioned above, we used only the wave function renormalization of the GBs, because we are interested in amplitudes without external Higgs particles. Thus it is not necessary to compute Z_h. With the methods described in the previous section, it is easy to calculate $Z_\phi - Z_h = \frac{B_1' - D'}{N}$. The inverse of the two point function matrix gives the propagators. As explained earlier, the diagonal GB propagators still have their pole at $s = 0$. One finds:

$$D_{hh}(s) = \frac{Z_\phi}{Z_h}\frac{1}{s - M^2(s)} \tag{33}$$

with

$$\frac{1}{M^2(s)} = \frac{1}{m^2(s)}\left\{1+\frac{1}{N}\Big[\frac{m^2(s)}{v^2}A(s) + 2C(s) + \frac{v^2}{m^2(s)}B(s)\Big]\right\}$$

The other propagators are:

$$\begin{aligned}
\frac{D_{h\chi}(s)}{D^0_{h\chi}(s)} &= \sqrt{\frac{Z_h}{Z_\phi}}\frac{D_{hh}(s)}{D^0_{hh}(s)} - \frac{1}{N}\Big[\frac{m^2(s)}{v^2}A(s) + C(s)\Big] \\
\frac{D_{\chi\chi}(s)}{D^0_{\chi\chi}(s)} &= \frac{Z_h}{Z_\phi}\frac{D_{hh}(s)}{D^0_{hh}(s)} - \frac{1}{N}\Big[\frac{m^2(s)}{v^2}A(s) - \frac{v^2}{s}B(s)\Big]
\end{aligned} \tag{34}$$

The three-point functions are:

$$\begin{aligned}
\Gamma_{h\pi\pi}(s) &= -\frac{2E(s)}{N} \\
\Gamma_{\chi\pi\pi}(s) &= -1 - \frac{F(s)}{N}
\end{aligned} \tag{35}$$

With these ingredients, one can express the amplitudes of the reactions $f\bar{f} \to f'\bar{f}'$ and $f\bar{f} \to zz$. Note that for any $Hf\bar{f}$ vertex one gets a multiplicative factor $\sqrt{Z_h/Z_\phi}$. The decomposition of the amplitudes into one-particle irreducible contributions is depicted in figure 8.

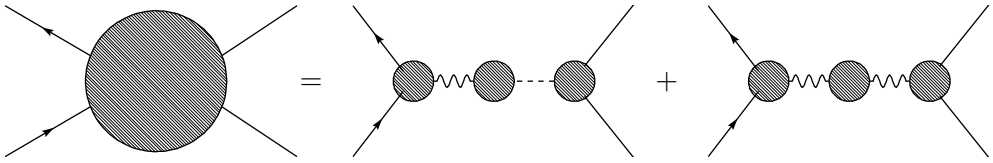

Figure 8: *Decomposition of the NLO 1/N corrections for the amplitude $\mathcal{M}(f\bar{f} \to zz)$ into irreducible vertex corrections and dressed propagators.*

$$\mathcal{M}(f\bar{f} \to f'\bar{f}') = \frac{1}{s - M^2(s)} \tag{36}$$

$$\mathcal{M}(f\bar{f} \to z\,z) = \frac{1}{s - M^2(s)} \frac{m^2(s)}{\sqrt{N} v} \times \left\{ 1 - \frac{1}{N} \Big[\frac{m^2(s)}{v^2} A(s) + C(s) + \frac{2v^2}{m^2(s)} E(s) + F(s) \Big] \right\} \tag{37}$$

The amplitudes can be measured directly at a future muon collider, and also can be related to Higgs production by gluon fusion at the LHC. The processes are available also to NNLO in usual perturbation theory, and thus are good quantities to compare the different theoretical approaches. One has simply to put $N = 4$ and $v = 123$ GeV in our formulae.

In figure 9 we plot the amplitudes of the two processes for several values of the coupling parameterized by m_h, defined in eq. 10. The Yukawa coupling is set to one. Note how the Higgs signal evolves from a sharp resonance to the damped regime, as the coupling is getting strong.

We compare our results with the perturbative ones in figure 10.

The peaks of the NLO $1/N$ and NNLO perturbation theory result are aligned to allow for a physically meaningful comparison between the two calculations. For on-shell Higgs masses below 1000 GeV the curves practically coincide. From this figure it is obvious that the results of both approaches agree with each other up to the highest accessible energies of the LHC. Away from the resonance, the perturbative curves which we give are not expected to be a good approximation. Close to the vector boson pair production threshold, the equivalence theorem is not valid anymore, and the curves will be modified by contributions of order of the vector boson masses.

As discussed in earlier publications [11], one finds in both approaches a saturation of the peak position. This is confirmed now also for the process $f\bar{f} \to zz$. The saturation effect is shown in figure 11.

It turns out that the NNLO perturbative result allows a maximal peak position of about 1100 GeV, whereas for the $1/N$ result one finds 975 GeV. In the case of $f\bar{f} \to f'\bar{f}'$ one finds 980 GeV for the perturbative and 930 GeV for the $1/N$ result. In this sense, the nonperturbative prediction is phenomenologically more restrictive.

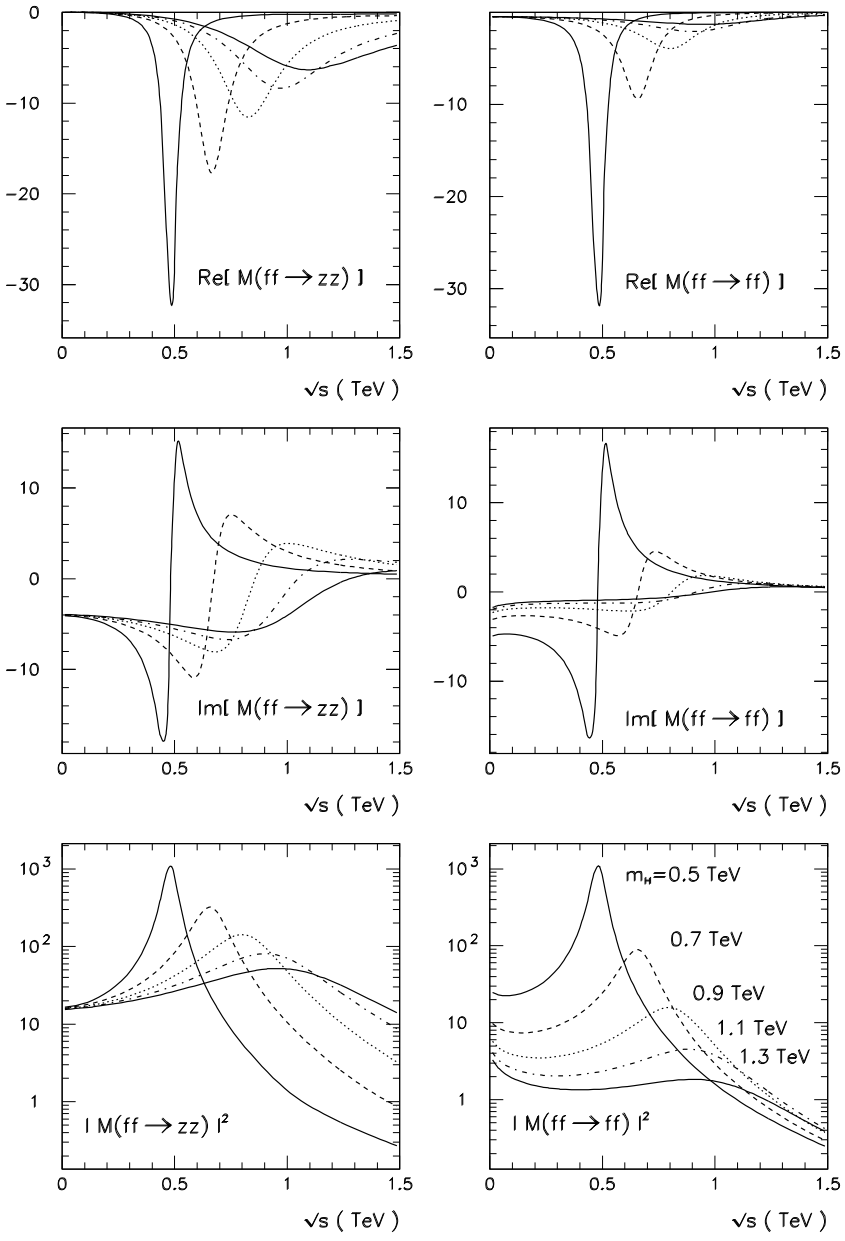

Figure 9: *Real, imaginary part and absolute square of the amplitude* $\mathcal{M}(f\bar{f} \to zz)$ *(left) and* $\mathcal{M}(f\bar{f} \to f'\bar{f}')$ *(right).*

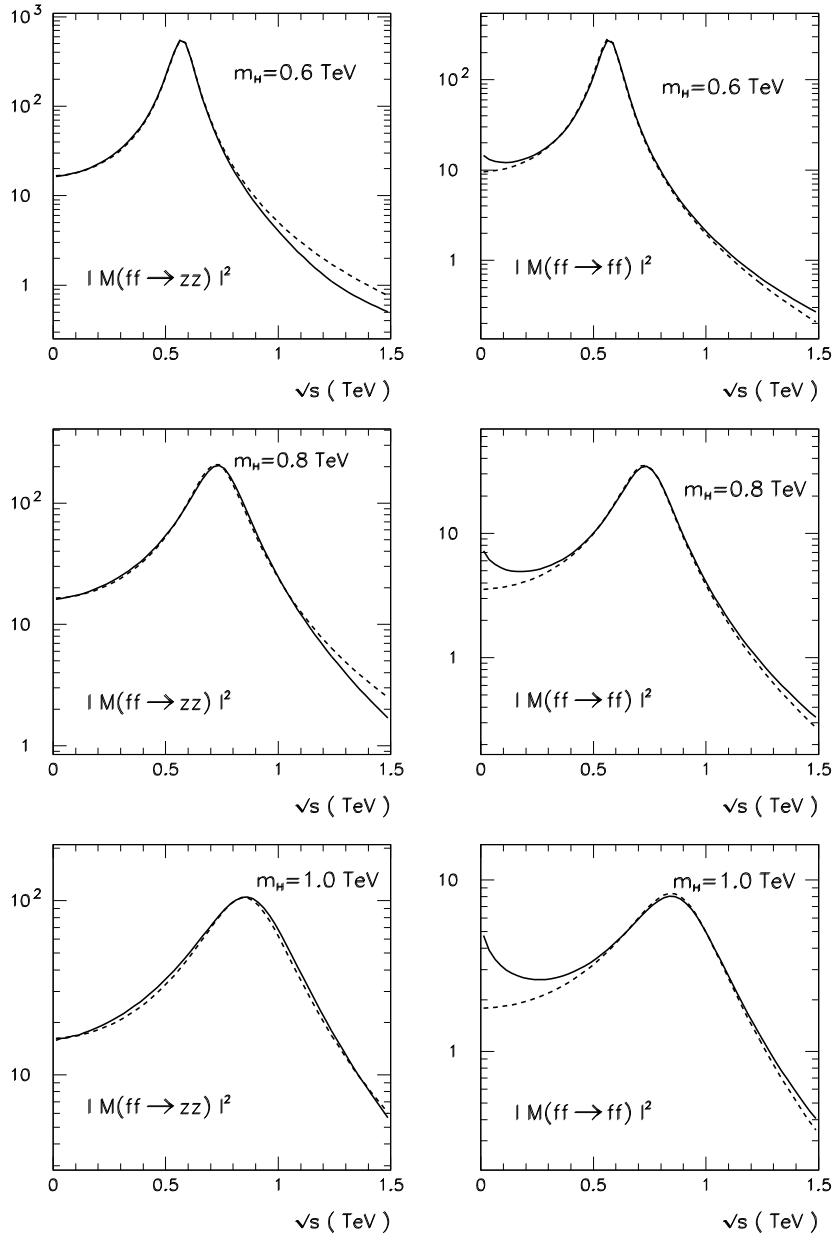

Figure 10: *Comparison between the line shapes computed in next-to-leading order* $1/N$ *(solid line) and two-loop perturbation theory (dashed line).*

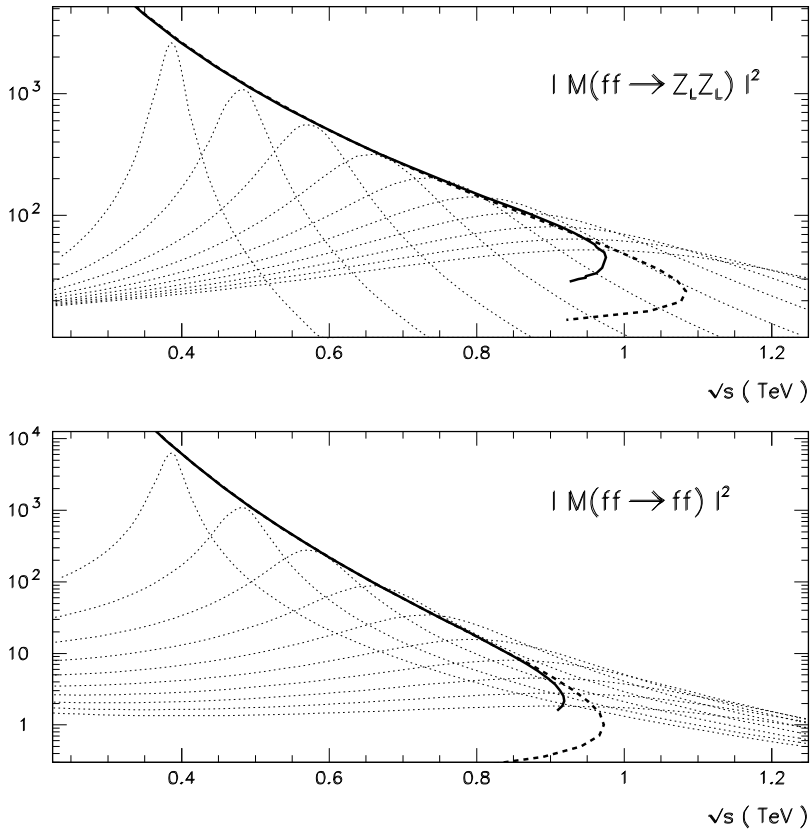

Figure 11: *The saturation effect of the Higgs resonance for the processes* $f\bar{f} \to zz$ *(a) and* $f\bar{f} \to f'\bar{f}'$ *(b). The solid and dashed curves are the position of the peak computed in the* $1/N$ *expansion and perturbation theory, respectively.*

5 Conclusions

We described in some detail the computation of Higgs production processes in the nonperturbative $1/N$ expansion for processes which are relevant for future colliders. We want to stress that our calculation reproduces the perturbative results in the region up to around $m_h = 800$ GeV in a very precise manner, which shows the consistency between perturbative methods and the $1/N$ expansion including our tachyon subtraction scheme. Once the calculational tools are developed, the calculation is not more difficult than a two-loop calculation in the Higgs sector. Beyond $m_h \sim 900$ GeV, there are differences between the $1/N$ expansion and perturbation theory concerning the position of the peak maxima, but the implications for Higgs-discovery physics are not too large up to ~ 1.1 TeV. This leads to the conclusion that the Higgs sector is theoretically well understood for the entire kinematic region relevant for Higgs searches at LHC [15].

A saturation of the peak position at strong coupling seems to be a general feature of a heavy Higgs boson.

Note that the $1/N$ approach disentangles the uncertainties from the renormalization scheme which is simply not present, from the cutoff effects due to the tachyonic pole. The effect of the tachyonic regularization becomes more important as the coupling is increased, modeling nondecoupling effects from a more fundamental theory containing the Higgs sector as an effective theory.

Appendix

The following formulae [13, 14] are used to get the integral representations of the $1/N$ graphs of eq. 29. With its help the appearing two- and three-loop topologies can be cast into the form of one-loop integrals.

Three-point massless scalar integral:

$$C_0(k^2,p^2,q^2) = \frac{1}{8\pi^2}\frac{1}{k^2\sqrt{\Delta}}\left[Li_2\Big(-\frac{u_2}{v_1}\Big) + Li_2\Big(-\frac{v_2}{u_1}\Big) + \frac{1}{4}\log^2\Big(\frac{u_2}{v_1}\Big) + \frac{1}{4}\log^2\Big(\frac{v_2}{u_1}\Big) + \frac{1}{4}\log^2\Big(\frac{u_1}{v_1}\Big) - \frac{1}{4}\log^2\Big(\frac{u_2}{v_2}\Big) + \frac{\pi^2}{6}\right] \tag{38}$$

with

$$\begin{aligned} u_{1,2} &= (1+b-a\pm\sqrt{\Delta})/2 \\ v_{1,2} &= (1-b+a\pm\sqrt{\Delta})/2 \\ \Delta &= 1-2(a+b)+(a-b)^2 \\ a &= p^2/k^2 \\ b &= q^2/k^2 \end{aligned}$$

Four-point massless scalar integral:

We use the notation $k_{ij} = -(\sum_{l=i}^{j-1} k_l)^2$ for the Mandelstam variables which are defined by the external momenta $k_{l=1,\ldots,4}$:

$$
\begin{aligned}
D_0(k_1,k_2,k_3) = D_0(k_{12},k_{13},k_{14},k_{23},k_{24},k_{34}) = \\
\frac{1}{(4\pi)^2 a(x_1-x_2)} \sum_{k=1}^{2} (-1)^k \Bigg\{ -\frac{1}{2}\log^2(-x_k) \\
-Li_2\Big(1+\frac{k_{34}-i\delta}{k_{13}-i\delta}x_k\Big) - \eta\Big(-x_k, \frac{k_{34}-i\delta}{k_{13}-i\delta}\Big)\log\Big(1+\frac{k_{34}-i\delta}{k_{13}-i\delta}x_k\Big) \\
-Li_2\Big(1+\frac{k_{24}-i\delta}{k_{12}-i\delta}x_k\Big) - \eta\Big(-x_k, \frac{k_{24}-i\delta}{k_{12}-i\delta}\Big)\log\Big(1+\frac{k_{24}-i\delta}{k_{12}-i\delta}x_k\Big) \\
+\log(-x_k)\Big[\log(k_{12}-i\delta)+\log(k_{13}-i\delta) \\
-\log(k_{14}-i\delta)-\log(k_{23}-i\delta)\Big]\Bigg\}
\end{aligned}
\tag{39}
$$

whereby,

$$
\begin{aligned}
x_{1,2} &= \frac{-b \pm \sqrt{b^2-4ac-4iad\delta}}{2a} \\
a &= k_{24}k_{34} \\
b &= k_{13}k_{24}+k_{12}k_{34}-k_{14}k_{23} \\
c &= k_{12}k_{13} \\
d &= k_{23} \\
\eta(u,v) &= \log(uv)-\log(u)-\log(v)
\end{aligned}
$$

The cut of the logarithm lies along the negative real axis. An infinitesimal replacement $i\delta$ is included to stay on the correct Riemann sheet if an argument vanishes.

Both formulae allow for analytical continuation of an external momentum which is important for our numerical purposes. This was checked by recalculating several known two-loop diagrams with the same methods as used for the computation of the 1/N graphs.

References

[1] B. A. Kniehl, Phys. Rept. 240, (1993) 211.

[2] W.J. Marciano and S.S.D. Willenbrock, Phys. Rev. D37 (1988) 2509.

[3] A. Ghinculov and J.J. van der Bij, Nucl. Phys. **B436** (1995) 30; A. Ghinculov, Nucl. Phys. B455 (1995) 21; Phys. Lett. B337 (1994) 137; (E) B346 (1995) 426.

[4] P. N. Maher, L. Durand and K. Riesselmann, Phys. Rev. D48 (1993) 1061; (E) D52 (1995) 553; L. Durand, B.A. Kniehl and K. Riesselmann, Phys. Rev. D51 (1995) 5007; Phys. Rev. Lett. 72 (1994) 2534; (E) Phys. Rev. Lett. 74 (1995) 1699; A. Frink, B.A. Kniehl, D. Kreimer, K. Riesselmann, Phys. Rev. D54 (1996) 4548.

[5] V. Borodulin and G. Jikia; Phys. Lett. B391 (1997) 434.

[6] G. Degrassi, P. Gambino, M. Passera and A. Sirlin, Phys. Lett. B418 (1998) 209.

[7] W. Langguth, I. Montvay, Z. Phys. C36 (1987) 725; A. Hasenfratz, T. Neuhaus, Nucl. Phys. B297 (1988) 205.

[8] S. Coleman, R. Jackiw, H.D. Politzer, Phys. Rev. D10 (1974) 2491;

[9] H.J. Schnitzer, Phys. Rev. D10 (1974) 1800; L. Dolan and R. Jackiw, Phys. ReV. D9 (1974) 3320.

[10] M.B. Einhorn, Nucl. Phys. B246 (1984) 75. R. Casalbuoni, D. Dominici and R. Gatto, Phys. Lett. B147 (1984) 419.

[11] A. Ghinculov, T. Binoth, J.J. van der Bij, Phys. Rev. D57 (1998) 1487; T. Binoth, A. Ghinculov, J.J. van der Bij, Phys. Lett. B417 (1998) 343.

[12] J.P. Nunes, H.J. Schnitzer, Int.J.Mod.Phys. A10 (1995) 719.

[13] A. Ghinculov, Phys. Lett. B385 (1996) 279.

[14] A. Denner, U. Nierste, R. Scharf, Nucl. Phys. B367 (1991) 637.

[15] A. Ghinculov, T. Binoth, J.J. van der Bij, Phys. Lett. B427 (1998) 343.